Nuclear Instruments and Methods in Physics Research A 342 (1994) 90–95
North-Holland

NUCLEAR
INSTRUMENTS
& METHODS
IN PHYSICS
RESEARCH
Section A

Capacitances in silicon microstrip detectors *

E. Barberis [a], N. Cartiglia [a], C. LeVier [a], J. Rahn [a], P. Rinaldi [a], H.F.-W. Sadrozinski [a,**], R. Wichmann [a], T. Ohsugi [b], Y. Unno [c], H. Miyata [d], N. Tamura [e], K. Yamamoto [f]

[a] *Santa Cruz Institute for Particle Physics, University of California, Santa Cruz, CA 95064, USA*
[b] *Hiroshima University, Higashi-Hiroshima 724, Japan*
[c] *KEK, Oho Tsukuba 305, Japan*
[d] *Niigata University, Niigata 950-21, Japan*
[e] *Okayama University, Okayama 700, Japan*
[f] *Hamamatsu Photonics K.K., Hamamatsu 435, Japan*

We present an analysis of the capacitances which are important for the operation of double-sided, AC-coupled silicon microstrip detectors. From frequency dependent measurements we extract interstrip, body and coupling capacitances of the strips, using SPICE simulations. Using electrostatic simulations we calculate the geometry dependence of interstrip and body capacitances and of depletion voltages. We evaluate the radiation hardness and the noise contribution of different strip geometries.

1. Introduction

In double-sided, AC-coupled silicon microstrip detectors, the signal to noise ratio is a function of detector capacitances: the coupling capacitance influences the signal strength, and the interstrip and body capacitances the noise level. In addition, the resistance of the metal strip can influence the signal strength for fast shaping.

One parameter which determines the capacitances is the geometry of the strips. We have pointed out before [1], that the interstrip capacitance is minimized with narrow strips. For the ohmic side where oxide charges cause a build-up of a conductive layer increasing the interstrip capacitance, it is possible to lower the interstrip capacitance with p-blocking strips [2]. In detectors with integrated AC-coupling, wide strips increase the coupling capacitance between the implant and the metal. This also decreases the resistance of the metal strip, which has to be minimized in order to reduce the dispersion of the signal [3].

In this paper we describe the extraction of capacitances on AC-coupled test detectors of various geometries by simulations of the frequency dependence of the measurements. We investigate the effect of the geometry on the value of the capacitances and the depletion voltage. We have measured the change of interstrip capacitances during radiation (p's and γ's) for different strip geometries. Finally we verified our understanding of the capacitance of various strip widths by measuring their effect on the noise of a fast amplifier–comparator chip. We comment on the influence of the metal strip resistance on the noise.

2. Experimental set-up

We have measured the interstrip, coupling and body capacitance as a function of strip and p-blocking implant width. AC-coupled test detectors were manufactured by Hamamatsu Photonics [4] in a program to determine the optimum geometric layout of double-sided silicon detectors for the SSC [5]. These are single-sided sample detectors of 50 μm pitch and 5.88 cm length with either junction or ohmic side processing on n-type bulk. Details can be found in refs. [6,7]. The implant of each strip is connected to a bus through a 460 kΩ polysilicon resistor and can be accessed via "DC" pads. The corresponding metal strip is isolated by a thin layer of silicon oxide (the coupling capacitor) and is connected to the "AC" pads on the other end.

Each sample detector is divided into four areas with different strip geometries: on the junction side, the strip width is varied; on the ohmic side the widths of the p-blocking strips are varied for constant width of the n-implant.

The measurements have been performed on both the AC and DC pads as function of frequency with a HP 4284A LCR meter. During the measurements the detectors were biased at normal operating conditions, (the p- (n-) implants were held at ground while the backplane was close to 100 (−100) V).

* Work supported in part by the U.S. Department of Energy, the Texas National Research Laboratory Commission, the US–Japan Collaborative Program, and the Joint Research of the International Scientific Research Program, Ministry of Education, Science and Culture, Japan.
** Corresponding author.

SSDI 0168-9002(93)E0942-L

3. Frequency dependence and SPICE simulations

The measured capacitances exhibit a strong frequency dependence due to the fact that the detectors act as an extended network of resistors and capacitors. The implant strip and the metal strip can be represented as a series of finite but small resistors with distributed capacitors to the other electrode, the neighboring strips and the back plane.

In order to extract the frequency independent capacitance per unit length, we simulated our set-up and the LCR meter with the network simulator SPICE. We divided the strips into unit cells, each consisting of two resistors for the top layer of aluminum and two resistors for the implant with capacitor bridges between them. Increasing the number of resistors per centimeter, we found convergence at high frequency with 64 cells/cm. Since we determined that the contributions from the neighboring strips far removed are small, the simulated model contains five strips: one central and four neighbors. Each implant strip is capacitively coupled to the top layer of aluminum, the conductive back plane, its two closest neighbors and its two second neighbors.

The goal of the SPICE simulations is to extract a frequency independent capacitance and resistance from the frequency dependent measurement. A more complete description of the simulation and the results is given in ref. [7].

4. Results of the extraction of capacitances

4.1. Coupling capacitance

The experimental and simulated results for the coupling capacitance of p-side detectors are plotted in Fig. 1. The resistivity of the implant could not be measured

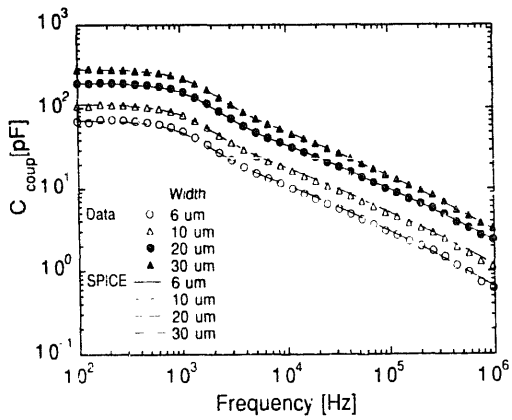

Fig. 1. Coupling capacitance for different p-strip widths as a function of frequency (measurements and SPICE simulation).

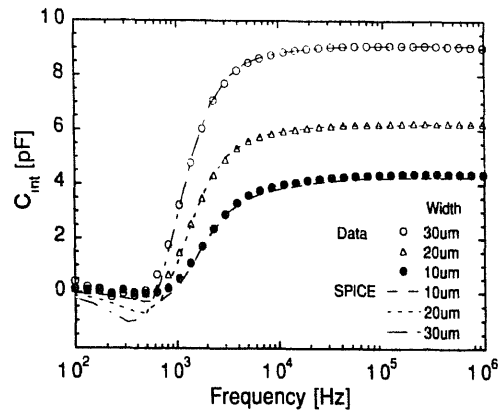

Fig. 2. AC interstrip capacitance for different p-strip widths as function of frequency (measurement and SPICE simulation).

directly, so SPICE was used to determine its value. The simulations agree very well with the data. The extracted coupling capacitance agrees with the low frequency limit of the measurement. At higher frequencies (> 1 kHz) only a small length of the p-implant contributes to the capacitance and thus the observed capacitance is reduced. The simulation also yields the value of the implant resistance for each of the four strip widths.

The values of the coupling capacitance per unit length (19 pF/cm) and the resistance for the p-implant (400 kΩ/cm), both for 10 μm strip width, scale well with implant width.

4.2. Interstrip capacitance

The interstrip capacitance is the main contributor to the noise. Because it is mainly a surface effect, we have to check carefully the behavior under ionizing radiation (see below). We have measured the interstrip capacitance using both the DC and AC pads of the p-side detectors. Fig. 2 shows the results for the AC interstrip capacitance between one metal strip and the four closest neighboring metal strips. Low frequencies are shunted to ground through the polysilicon resistors resulting in a high pass filter: the values for the AC interstrip capacitance extracted from SPICE are therefore close to the high frequency values of Fig. 2.

4.3. Body capacitance

The body capacitance of one strip to the backplane is important because we use its voltage dependence to determine the depletion voltage. We have measured the body capacitance of the whole p-side detector placing one of the two terminals on the bus and the other on the backplane and over-depleting the detector. The measured values agree with the simulation as shown in Fig. 3. We can illustrate the necessity of

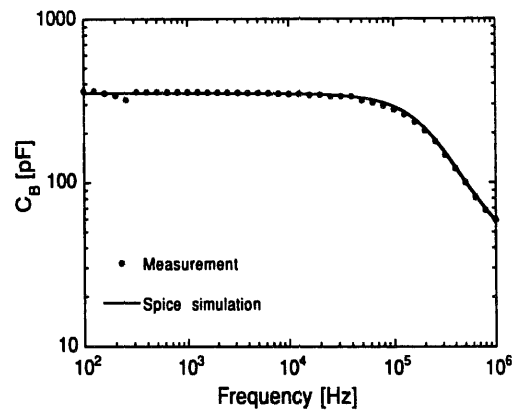

Fig. 3. Body capacitance after depletion for a p-type detector as a function of frequency (measurement and SPICE simulation).

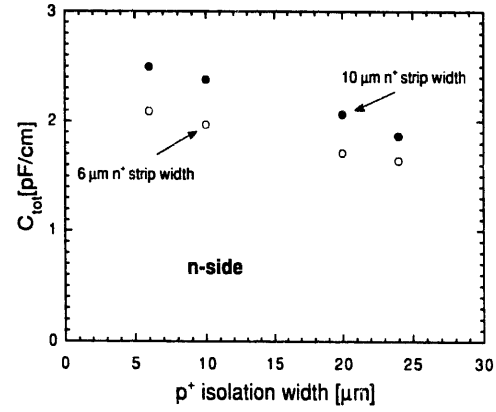

Fig. 5. Total capacitance for a 50 μm pitch n-side silicon detector as a function of p^+ isolation width for strip widths of 6 and 10 μm.

mapping out the frequency dependence of the capacitance instead of measuring only at one frequency: at 100 kHz, the body capacitance is only 83% of the extracted value.

4.4. Total capacitance

We have determined the total interstrip capacitance as the sum of the measured AC interstrip capacitance to the first two pairs of neighbors plus a small correction, 0.1 pF/cm, due to the presence of all the remaining strips. The total capacitance is then the sum of the total interstrip capacitance and the body capacitance.

The total capacitance for p-side silicon detectors with different strip width but constant strip pitch of 50 μm is shown in Fig. 4 as function of the ratio strip width over pitch w/p. The results are compared with the theoretical prediction obtained solving numerically for the electric field inside the detector [1]. The data agree with the simulations, indicating that the p-side capacitance is given by the geometric capacitance alone.

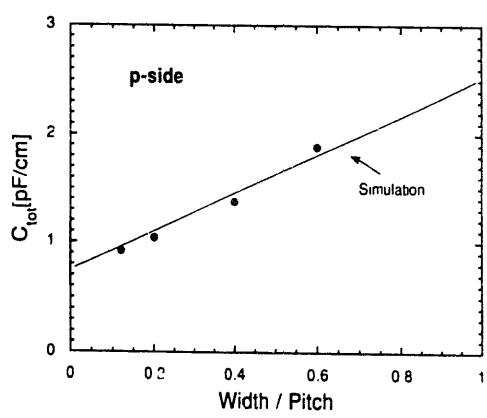

Fig. 4. Total capacitance for a 50 μm pitch p-side detector as a function of the ratio width over pitch w/p.

We emphasize again that a reduced strip width lowers the total capacitance.

Fig. 5 shows the total capacitance for n-side detectors with 6 and 10 μm strip width as a function of the width of the p-blocking strip. For n-side detectors, wider p^+ isolation implants and narrower n-implants reduce the capacitance. We observe somewhat higher capacitances than on the p-side, suggesting the presence of free charges close to the surface which can be removed with higher fields, evident in the fact that the interstrip capacitance decreases with increasing bias voltage beyond depletion.

5. Radiation damage

We have irradiated the sample detectors with gamma rays from a ^{60}Co source and with 650 MeV protons with total doses of up to 8.5 Mrad [8,9]. During irradiation the backplane and the metal strip were held at ground while the p- (n-) implants were biased at −80 (+80) V, respectively. Here we will only discuss the change in interstrip capacitance. The coupling capacitance was shown to be stable [9] and the bulk effects leading to a change in the depletion voltage are discussed in ref. [10].

We determined the AC interstrip capacitance to the next four neighbors for both the junction and ohmic side as a function of the total dose, choosing the high frequency limit at 1 MHz (cf. Fig. 2). The results are shown for the p-side in Fig. 6 for different p-implant widths. First we collected a gamma dose of 5 Mrad. We see that the interstrip capacitance is nearly constant for small strip width and increases with radiation for wide strip width (20 μm). After gamma irradiation, we added protons with a fluence of about 10^{14} p/cm^2 for a total dose of 8.5 Mrad. During the proton irradiation, the n-bulk inverted [11], causing the junction to

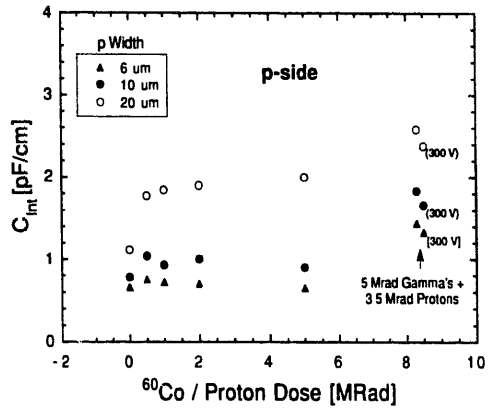

Fig. 6. p-side interstrip capacitance to 1st and 2nd neighbors as a function of dose for different p-strip widths. The first 5 Mrad were accumulated with gamma's, and then 3.5 Mrad of high energy protons were added. At the dose of 8.5 Mrad, the capacitances were measured at bias voltages of 200 and 300 V.

move to the n-side: depletion is now starting from the n-side. We conclude from Fig. 6 that the interstrip capacitance is increased after inversion and moreover exhibits a dependence on the bias voltage: when we raise it from 200 V (the depletion voltage) to 300 V, the capacitance decreases. This voltage dependence is similar to the interstrip capacitance on the ohmic side before irradiation, which we attributed to insufficient removal of all free charges between the strips.

In Fig. 7, we show the interstrip capacitance for the n-side for different p^+ blocking strip widths and an n-implant width of 10 μm as a function of γ dose and for a separate proton irradiation with 10^{14} p/cm^2. We find that gamma irradiation does not change the interstrip capacitance, at least for detectors with wide p^+ isolation. After inversion, i.e., after proton irradiation,

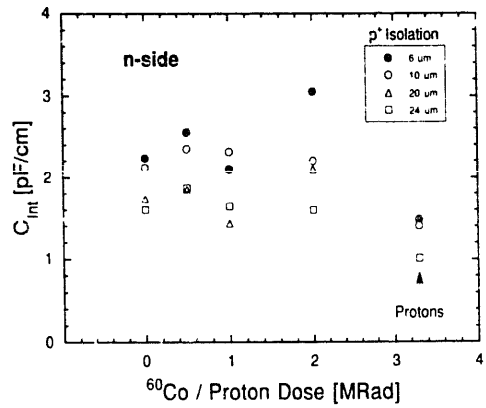

Fig. 7. n-side interstrip capacitance to 1st and 2nd neighbors as a function of dose for various p^+ isolation widths (implant width 10 μm). The 2.2 Mrad gamma's and the 3.5 Mrad high energy protons were supplied to different detectors.

the interstrip capacitance drops for all geometries to below the prerad levels. Moreover, no dependence on the bias voltage is observed, very much like on the p-side before inversion. These facts are consistent with our hypothesis that insufficient removal of free charges in low electric fields on the ohmic side cause an increase in interstrip capacitance.

6. Geometry dependence of the depletion voltage and the body capacitance

Novel designs of detectors with varying strip pitch p and/or width w ("wedged" detectors, see ref. [12]) pose the question how depletion voltage and body capacitance depend on the strip geometry. We have investigated this dependence using the electrostatic simulation program of ref. [1], and present here only the results; details can be found in ref. [13]. For a planar diode of thickness d, the bias voltage V_{Bias} is proportional to the square of the depletion depth x:

$$V_{Bias} = \frac{\epsilon N}{2e} x^2, \tag{1}$$

and the body capacitance per unit length c_B is inversely proportional to x:

$$c_B = \frac{C_B}{l} = \epsilon \frac{p}{x} = \epsilon \frac{p}{d} \sqrt{\frac{V_{D0}}{V_{Bias}}}. \tag{2}$$

Thus, the capacitance of a planar diode exhibits a $V_{Bias}^{-1/2}$ behavior before the bias voltage reaches the depletion voltage V_{D0}. For $V_{Bias} > V_{D0}$, the body capacitance per unit length is:

$$c_0 = \epsilon \frac{p}{d} = \text{const.} \tag{3}$$

The effect of the finite pitch and width of a strip detector is twofold: an increase in depletion voltage V_D and a decrease in body capacitance c_B. For junction-side, single-sided detectors, the increase in depletion voltage is caused by the fact that the equi-potential lines are encircling the strips and are getting parallel to the surfaces only at the depth of about the pitch p. The depletion voltage of the strip detector is increased to:

$$V_D = V_{D0}\left[1 + 2\frac{p}{d} f\left(\frac{w}{p}\right)\right], \tag{4}$$

and the capacitance per unit length is:

$$c_B = \epsilon \frac{p}{x + pf\left(\frac{w}{p}\right)} = \epsilon \frac{p}{d} \sqrt{\frac{V_{D0}}{V_{Bias} + V_{D0}\left[\frac{p}{d} f\left(\frac{w}{p}\right)\right]^2}}, \tag{5}$$

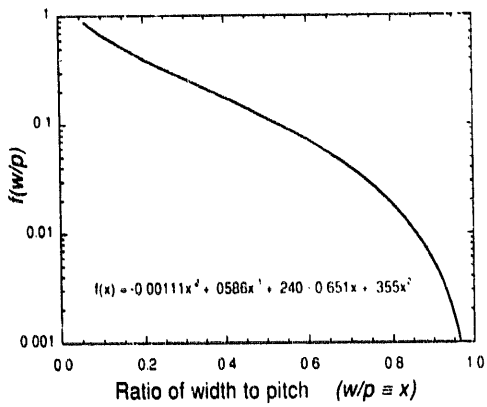

Fig. 8. Function $f(w/p)$ of eqs. (4), (5) and (6).

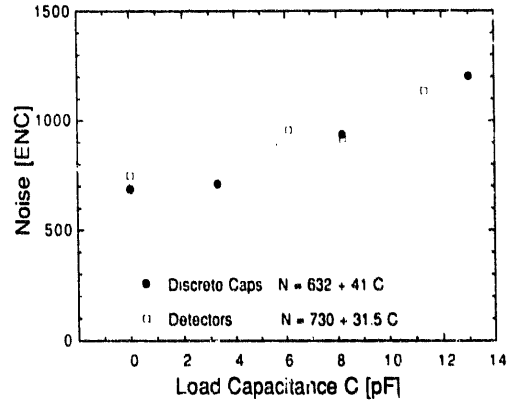

Fig. 9. Noise (in electrons) of an amplifier–comparator chip with 30 ns rise time as a function of load capacitance. External discrete capacitors and total strip capacitances of detectors with different strip width are compare

which results in a body capacitance at depletion c_{D}:

$$c_{\mathrm{D}} = \epsilon \frac{p}{d + pf\left(\frac{w}{p}\right)}. \tag{6}$$

The universal function $f(w/p)$ is shown in Fig. 8.

As an example, we calculate the depletion voltages for a single-sided wedged detector of 300 μm thickness, constant width of 9 μm and a pitch varying from 30 to 90 μm. Table 1 shows the ratios $V_{\mathrm{D}}/V_{\mathrm{D0}}$ and c_{D}/c_0 of strip depletion voltages and body capacitances relative to those of planar diodes, respectively. Compared to a planar diode of the same thickness, the depletion voltage is increased by 8% to 39%, and the capacitance after depletion is decreased by 2% to 16%. The junction side will have a c–V depletion curve shallower than $V_{\mathrm{Bias}}^{1/2}$ (cf. eq. (5)), while the ohmic side will deplete like a planar diode until the depletion depth is equal to the thickness, followed by a drop in capacitance due to the depletion between the n-strips.

In a trivial extension, we derive for double-sided detectors (of width w and w' for the p-side and n-side, respectively) the depletion voltage (cf. eq. (4)):

$$V_{\mathrm{D}} = V_{\mathrm{D0}}\left\{1 + 2\frac{p}{d}\left[f\left(\frac{w}{p}\right) + f\left(\frac{w'}{p}\right)\right]\right\}, \tag{7}$$

Table 1
Depletion voltages and body capacitances for single-sided detectors with varying pitch

Width w [μm]	Pitch p [μm]	$f(w/p)$ (Fig. 8)	$V_{\mathrm{D}}/V_{\mathrm{D0}} = 1 + 2\frac{p}{d}f(\frac{w}{p})$	$c_{\mathrm{D}}/c_0 = [1 + \frac{p}{d}f(\frac{w}{p})]^{-1}$
9	30	0.260	1.08	0.98
9	60	0.482	1.19	0.91
9	90	0.642	1.39	0.84

and the body capacitance at depletion (cf. eq. (6)):

$$c_{\mathrm{D}} = \epsilon \frac{p}{d + p\left[f\left(\frac{w}{p}\right) + f\left(\frac{w'}{p}\right)\right]}. \tag{8}$$

7. Noise

The total strip capacitance plays an important role since it contributes to the noise of the front-end amplifier. One can ask the question if a complicated network like a detector behaves like a simple capacitative load. We have measured the noise of a low noise amplifier–comparator chip with 30 ns rise time [14] with either discrete capacitors or silicon strip detectors of different width as load.

Fig. 9 shows the noise of the amplifier as function of load capacitance. In one case, the capacitances are given by external discrete components, while in the other they are presented by p-strips of different width, whose capacitance values can be taken from Fig. 4. The two noise curves are nearly identical, which leads us to conclude that the total strip capacitance generates noise like a discrete capacitor. The finite resistance of the metal strip (30 Ω/cm for 10 μm width) does not contribute to the noise of the fast amplifier. On the other hand, we have shown before [3] that the signal-to-noise ratio S/N is deteriorating with finite metal resistance much greater than 30 Ω/cm because the RC time constant of the transmission increases and the ballistic deficit (see ref. [15]) increases. A detailed SPICE simulation supports this conclusion [16].

8. Conclusion

We have measured the parasitic and coupling capacitances of AC-coupled silicon strip detectors. The

frequency dependence of the measurement can be simulated with SPICE and is understood in terms of a network of distributed capacitors and resistors.

We found that the parasitic capacitances are minimized with narrow implant widths on both readout sides and wide p^+ isolation strips on the n-side. These geometries are measured to be also relatively radiation hard.

Using electrostatic simulations, we have derived the geometry dependence of depletion voltage, and body and interstrip capacitances of strip detectors.

From noise measurements with a fast, low-noise amplifier connected to various strip geometries, we conclude that only the parasitic capacitance of the strips contributes to the noise, while the finite resistance deteriorates the signal transmission along the strip.

The optimization of the geometry of double-sided sensors is a challenge for the manufacturers: the width of implant and metal has to be decreased to minimize parasitic capacitances but increased to maximize the coupling capacitance and minimize the resistance; the oxide layer thickness has to be decreased to maximize the coupling capacitance, but increased to maximize the breakdown voltage.

Acknowledgments

We would like to thank W.A. Rowe, E. Spencer, A. Webster and M. Wilder for technical help and fruitful discussions.

References

[1] R. Sonnenblick et al., Nucl. Instr. and Meth. A 310 (1991) 189.
[2] R. Yamamoto, Proc. SDC Collaboration Meeting at KEK, SDC-91-33 (1991).
[3] W. Gadomski et al., Nucl. Instr. and Meth. A 326 (1993) 239.
[4] Hamamatsu Photonics K.K., Hamamatsu City, Japan.
[5] T. Ohsugi, these Proceedings (Int. Symp. on Development and Application of Semiconductor Tracking Detectors, Hiroshima, Japan, 1993) Nucl. Instr. and Meth. A 342 (1994) 16.
[6] E. Barberis et al., IEEE Nucl. Sci. Symp., Orlando, FL, 1992, Santa Cruz Institute for Particle Physics SCIPP 92/14.
[7] C. LeVier, UC Santa Cruz Senior thesis, Santa Cruz Institute for Particle Physics SCIPP 92/26.
[8] H. Ziock et al., IEEE Trans. Nucl. Sci. NS-37 (1990) 1238.
[9] D. Pitzl et al., Nucl. Phys. B (Proc. Suppl.) 23 A (1991) 340.
[10] H. Ziock et al., ref. [5], p. 96.
[11] D. Pitzl et al., Nucl. Instr. and Meth. A 311 (1992) 98.
[12] J. Krismanic, ref. [5], p. 27.
[13] J. Rahn, Santa Cruz Institute for Particle Physics SCIPP 93/12.
[14] E. Barberis et al., Proc. 3rd Int. Conf. on Advanced Technology and Particle Physics, Como, Italy, 1992, Nucl. Phys. B (Proc. Suppl.) 32 (1993) 513.
E. Barberis et al., IEEE Trans. Nucl. Sci. NS-40 (1993) 740.
[15] D. Dorfan, ref. [5], p. 143.
[16] E. Spencer and M. Wilder, Santa cruz Institute for Particle Physics SCIPP 93/15.